INTERNATIONAL JOURNAL FOR NUMERICAL METHODS IN FLUIDS, VOL. 7, 1035–1052 (1987)

A FINITE ELEMENT PROCEDURE FOR VISCOELASTIC FLOWS

M. FORTIN AND D. ESSELAOUI

Université Laval, Québec, GIK 7P4, Canada

SUMMARY

A finite element method for the simulation of viscoelastic flows has been developed. It uses a weak formulation of the method of characteristics to treat the viscoelastic constitutive law. Numerical results in a 4:1 contraction are presented and are discussed with respect to previous computations. New phenomena are put in evidence and new questions are opened in this already controversial problem.

KEY WORDS Non-Newtonian Flows Viscoelasticity Maxwell Fluids

INTRODUCTION

We shall describe in this paper a numerical method for the simulation of viscoelastic fluids. These fluids are a special case of non-Newtonian fluids that lie somewhere in between elastic materials and standard Newtonian fluids.

This class, as all classes defined negatively, contains many different things. The general framework is continuum mechanics, from which we recall a few facts. We consider a flow in a domain Ω of $\mathbb{R}^2$ or $\mathbb{R}^3$; a flow is described first by the velocity field $\mathbf{u}(\mathbf{x})$, $\mathbf{x}\in\Omega$. We shall suppose in the following that we deal with an incompressible material of constant density so that conservation of mass reduces to the divergence-free condition

$$\operatorname{div}\mathbf{u}=0. \tag{1}$$

The second general law will be conservation of momentum, that becomes in the steady-state case equilibrium of forces. To write it, we need the stress tensor $\boldsymbol{\sigma}$. We then have

$$\rho\left(\frac{\partial\mathbf{u}}{\partial t}+\mathbf{u}\cdot\nabla\mathbf{u}\right)-\operatorname{div}\boldsymbol{\sigma}=\rho\mathbf{f}, \tag{2}$$

where ρ is the density of the fluid and $\mathbf{f}$ summarizes external forces. The operator ∇ is the gradient operator. It is defined by

$$(\nabla\mathbf{u})_{ij}=\frac{\partial u_i}{\partial x_j}. \tag{3}$$

In many cases we shall neglect in (2) the inertial terms $\mathbf{u}\cdot\nabla\mathbf{u}$ to use the creeping-flow approximation

$$\rho\frac{\partial\mathbf{u}}{\partial t}-\operatorname{div}\boldsymbol{\sigma}=\rho\mathbf{f}. \tag{4}$$

Based on an invited lecture.

0271–2091/87/101035–18$09.00
© 1987 by John Wiley & Sons, Ltd.

To complete this set of equations we need one more. This will be the constitutive law. This law is special to the *material* considered. In some cases it will even be restricted to a given material and a class of flows, because no general law is available to take into account all situations. Non-Newtonian flows will thus be characterized and differentiated by their constitutive law, which will be some relation between the stress tensor and other properties of the flow. The classical Newtonian law is simply

$$\boldsymbol{\sigma}^{\mathrm{D}} = 2\mu \mathbf{D}(\mathbf{u}), \tag{5}$$

where $\boldsymbol{\sigma}^{\mathrm{D}} = \boldsymbol{\sigma} - [\operatorname{tr}(\boldsymbol{\sigma})/n]\mathbf{I}$ is the deviatoric of the stress tensor $\boldsymbol{\sigma}$, $n = 2$ or 3 is the dimension of the space and $\mathbf{D}(\mathbf{u})$, the strain rate tensor, is the symmetric tensor

$$\mathbf{D}(\mathbf{u}) = \tfrac{1}{2}[(\nabla \mathbf{u}) + (\nabla \mathbf{u})^{\mathrm{T}}]. \tag{6}$$

From this point many variations are possible. We shall describe briefly in the next section the case of generalized Newtonian fluids, where the viscosity μ will be supposed to be dependent on $\mathbf{D}(\mathbf{u})$.

Finally we shall consider a class of viscoelastic flows in which the stress tensor will depend on its own history; that is, a memory effect will be involved in the description of the material.

We shall try to build a numerical method that will degenerate in the Newtonian case to a simple and proven method. Moreover, following a technique that was successful for generalized Newtonian flows, we shall try to restrict all computations related to constitutive laws to element level. Numerical results show that this technique yields interesting new facts. We apologize that it is of course not possible in a short paper to review the full literature on such a wide subject. We refer the reader to the comprehensive study of Crochet *et al.*[1] for a more general presentation.

GENERALIZED NEWTONIAN FLOWS

We recall in this section a numerical method for the treatment of a large class of relatively simple fluids, which are often termed as generalized Newtonian fluids. The reader may refer to References 2 and 3 for further details. The fluids that we now consider are characterized by a viscosity depending on the second invariant of the strain rate tensor. Precisely, we suppose a constitutive law of the form,

$$\boldsymbol{\sigma}^{\mathrm{D}} = 2\eta(|\mathbf{D}(\mathbf{u})|^2)\mathbf{D}(\mathbf{u}). \tag{7}$$

Generally $\eta(\cdot)$ is a scalar, but it would be possible to introduce a matrix in order to model anisotropic behaviours appearing in certain polymeric liquids. A widely used law of the form (7) is the simple power law,

$$\boldsymbol{\sigma}^{\mathrm{D}} = 2\mu|\mathbf{D}(\mathbf{u})|^{p-2}\mathbf{D}(\mathbf{u}). \tag{8}$$

In (7) and (8), $|\mathbf{D}(\mathbf{u})| = (\sum D_{ij}^2(\mathbf{u}))^{1/2}$ is the second invariant of the strain rate tensor. Supposing now η to be a scalar monotonic function of $|\mathbf{D}(\mathbf{u})|^2$ we introduce the functional,

$$J(\mathbf{v}) = \int \phi(|\mathbf{D}(\mathbf{v})|^2)\,\mathrm{d}x - \int_\Omega \mathbf{f}\cdot\mathbf{v}\,\mathrm{d}x, \tag{9}$$

where $\phi'(s) = \eta(s)$. Minimizing $J(\mathbf{v})$ over a suitable divergence-free vector field (that depends on the particular function ϕ considered), one obtains the solution of the non-linear creeping flow problem:

$$\operatorname{div}[\eta(|\mathbf{D}(\mathbf{u})|^2)\mathbf{D}(\mathbf{u})] = \mathbf{f}, \tag{10}$$

$$\operatorname{div}\mathbf{u} = 0, \tag{11}$$

with boundary conditions associated with the choice of the functional space.

We now briefly recall an algorithm that will permit a local (element-wise) treatment of the non-linearity. This will afterwards be used as a guideline for further developments to viscoelastic materials. The trick in the present case is to transform our minimization problem into a saddle-point problem by introducing an auxiliary variable $\mathbf{q}$ that should be equal, when the solution is found, to $\mathbf{D}(\mathbf{u})$. We thus write the *augmented Lagrangian* problem:

$$\operatorname*{Inf\,sup}_{\mathbf{q},\mathbf{v}\ \ \lambda} \int_\Omega \phi(|\mathbf{q}|^2)\,dx - \int_\Omega \mathbf{f}\cdot\mathbf{v}\,dx + \int_\Omega \lambda{:}(\mathbf{q}-\mathbf{D}(\mathbf{v}))\,dx + \frac{r}{2}\int_\Omega a(x)(\mathbf{q}-\mathbf{D}(\mathbf{v}))^2\,dx. \tag{12}$$

The solution of this is now characterized by the system

$$r\int_\Omega a(x)\mathbf{D}(\mathbf{u}){:}\mathbf{D}(\mathbf{v})\,dx - \int_\Omega [\lambda + ra(x)\mathbf{P}]{:}\mathbf{D}(\mathbf{v})\,dx = \int_\Omega \mathbf{f}\cdot\mathbf{v}\,dx, \forall \mathbf{v}, \tag{13}$$

$$\int_\Omega [\eta(|\mathbf{D}(\mathbf{u})|^2) + ra(x)\mathbf{p}{:}\mathbf{q}\,dx - \int_\Omega [ra(x)\mathbf{D}(\mathbf{u}) - \lambda]{:}\mathbf{q}\,dx = 0, \forall \mathbf{q}, \tag{14}$$

$$\mathbf{P} = \mathbf{D}(\mathbf{u}). \tag{15}$$

We recall that the space V should be a space of divergence-free functions. An algorithm to solve this system is described in Reference 3, and for this particular case in Reference 2. It implies solving in sequence the *linear problem* (13) for $\mathbf{u}, \mathbf{p}$ and λ being given and then the non-linear problem (14) in $\mathbf{p}, \mathbf{u}$ and λ being given, those steps being used in an updating mechanism for λ.

Problem (14) contains no derivatives of $\mathbf{p}$. It can be solved pointwise. For a discretized problem this will mean at element level and even, if a proper choice of degrees of freedom is done, at a few Gaussian nodes on each element. Let us briefly describe the finite element discretization that was used. We used for the velocity and pressure components the now standard Q_2–P_1 approximation (Figure 1). We wanted our model to degenerate to a standard Newtonian model when viscosity was constant. This imposed that the approximations of λ and $\mathbf{p}$ should contain $\mathbf{D}(\mathbf{v}_h)$ for any discrete velocity field. This meant using at least an incomplete Q_2 approximation for each component of the tensors. In order to be able to build an orthogonal basis that permitted us to reduce computations to pointwise ones we approximated λ and $\mathbf{p}$ by complete Q_2 elements with Gaussian points as nodes (Figure 2).

This approximation is discontinuous, which is consistant with the augmented Lagrangian formulation and its decomposition properties.

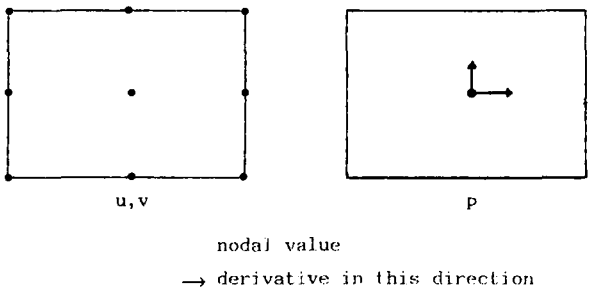

Figure 1. Velocity and pressure

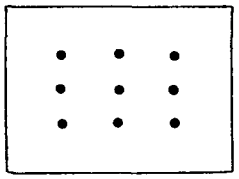

Figure 2. Tensors λ and $\mathbf{p}$

The success of this method led us to try to use analogue ideas for viscoelastic flows even if no such simple construction is obvious. We shall describe our solution method in the next section.

VISCOELASTIC FLOWS

We shall now try to build approximations for a more complex class of non-Newtonian flows, namely viscoelastic flows. We would like to do so in the same spirit as in the discretization of generalized Newtonian flows, that is:

(a) our approximations should reduce to a standard approximation of the Navier–Stokes equations when applied to a Newtonian flow
(b) treatment of the non-linearities introduced by constitutive equations should be kept at a local level.

This goal will be met by using a method of characteristics to deal with memory effects. But let us first describe the models we would like to consider.

Viscoelastic constitutive models

The difference between viscoelastic models and those proposed in the last section lies mainly in the introduction into the constitutive laws of *memory effects*. We shall no longer relate the stress tensor to the strain-rate tensor through some more or less complicated function, but rather write an evolution equation for stress or some of its components. We cannot present here the developments that lead to the constitutive laws described below; we refer the reader References 2–6, among others, for a general presentation. Let us merely recall that a fundamental point in building a model is *frame invariance*: the behaviour of a fluid should not depend on the co-ordinate system in which we write its equations. This requisite leads us to introduce the notion of convective derivatives for a tensor $\mathscr{T}$:

$$\frac{\delta_\theta}{\delta t}\mathscr{T} = \frac{\partial \mathscr{T}}{\partial t} + \mathbf{u}\cdot\nabla\mathscr{T} + [\mathscr{T}\,\boldsymbol{\Omega}(\mathbf{u}) - \boldsymbol{\Omega}(\mathbf{u})\mathscr{T}] + \theta[\mathscr{T}\,\mathbf{D}(\mathbf{u}) + \mathbf{D}(\mathbf{u})\mathscr{T}]. \tag{16}$$

For $\theta = 0$ we have the Jaumann derivative, which takes into account translation and rotation of a volume element of the flow. $\boldsymbol{\Omega}(\mathbf{u}) = \frac{1}{2}((\nabla\mathbf{u} - \nabla\mathbf{u})^{\mathrm{T}})$ is the vorticity tensor.

For $\theta = 1$ and $\theta = -1$ we obtain the covariant and contravariant derivatives, respectively,

$$\frac{\delta_1}{\delta t}\mathscr{T} = \frac{\partial \mathscr{T}}{\partial t} + (\mathbf{u}\cdot\nabla)\mathscr{T} + [\mathscr{T}(\nabla\mathbf{u}) + (\nabla\mathbf{u})^{\mathrm{T}}\mathscr{T}], \tag{17}$$

$$\frac{\delta_{-1}}{\delta t}\mathscr{T} = \frac{\partial \mathscr{T}}{\partial t} + [\mathbf{u}\cdot\nabla)\mathscr{T} - [(\nabla\mathbf{u})\mathscr{T} + \mathscr{T}(\nabla\mathbf{u})^{\mathrm{T}}]. \tag{18}$$

We now consider a special case of the eight-parameter Oldroyd model.[4] Now $\boldsymbol{\sigma}$ will be an *extra-*

stress and no longer a deviatoric. It is a solution of the equation

$$Y(\varepsilon,\boldsymbol{\sigma})\boldsymbol{\sigma}+\lambda_1\frac{\delta_\theta}{\delta t}\boldsymbol{\sigma}=2\eta_0[\mathbf{D}(\mathbf{u})+\lambda_2\frac{\delta_\xi}{\delta t}\mathbf{D}(\mathbf{u})]. \tag{19}$$

The cases $Y(\varepsilon,\boldsymbol{\sigma})\equiv 1, \lambda_2=0, \lambda_1$ and η_0 constants correspond to the usual Maxwell models of type A or B (covariant or contravariant models). The case $\lambda_2=0$ corresponds to the model of Phan Thien and Tanner.[7] Taking $\lambda_2\neq 0$ generalizes the so-called three-parameter Oldroyd model. This model is now used to define the stress tensor $\mathscr{T}$ of (2) by

$$\mathscr{T}=-p\mathbf{I}+\boldsymbol{\sigma}. \tag{20}$$

Following for instance Keunings and Crochet[8,15] we can simplify (19) to bring us back to the case $\lambda_2=0$. Let us indeed set

$$\boldsymbol{\sigma}=\boldsymbol{\sigma}_1+\boldsymbol{\sigma}_2, \tag{21}$$

where we have

$$\boldsymbol{\sigma}_2=2\eta_2\mathbf{D}(\mathbf{u}), \tag{22}$$

with $\eta_2=\eta_0(\lambda_2/\lambda_1)$ and $\eta_0=\eta_1+\eta_2$. In the case $Y(\varepsilon,\boldsymbol{\sigma})\equiv 1$ it is readily verified that (19) reduces to

$$\boldsymbol{\sigma}_1+\lambda_1\frac{\delta_\theta}{\delta t}\boldsymbol{\sigma}_1=2\eta_1\mathbf{D}(\mathbf{u}). \tag{23}$$

For the non-linear case $Y(\varepsilon,\boldsymbol{\sigma})=\exp((\varepsilon\lambda_1/\eta_0)\operatorname{tr}\boldsymbol{\sigma})$ this can no longer be done. However there is no real reason to believe that the following final model is less valid than the above one. We summarize therefore our problem in the equations

$$\rho\left(\frac{\partial\mathbf{u}}{\partial t}+\mathbf{u}\cdot\nabla\mathbf{u}\right)-\operatorname{div}\mathscr{T}=\rho\mathbf{f}, \tag{24}$$

$$\operatorname{div}\mathbf{u}=0, \tag{25}$$

$$\mathscr{T}=\boldsymbol{\sigma}_1+\boldsymbol{\sigma}_2-p\mathbf{I}, \tag{26}$$

$$Y(\varepsilon,\boldsymbol{\sigma}_1)\boldsymbol{\sigma}_1+\lambda_1\frac{\delta_\theta}{\delta t}\boldsymbol{\sigma}_1=2\eta_1\mathbf{D}(\mathbf{u}), \tag{27}$$

$$\boldsymbol{\sigma}_2=2\eta_2\mathbf{D}(\mathbf{u}). \tag{28}$$

This model contains the standard covariant and contravariant models, the model of Phan Thien and Tanner and the three-parameter Oldroyd model. If η_1 and λ_1 depend on $|\mathbf{D}(\mathbf{u})|$ it also contains the White–Metzner model.[8] In order to obtain a numerical method for this model we shall first introduce a Lagrangian formulation of (27).

Lagrangian form of the constitutive law

Referring to definition (16) one sees that the model (24)–(28) is non-linear and that it must be solved as a system: it is not possible to obtain a closed form for $\boldsymbol{\sigma}_1$ in order to eliminate this unknown. We shall however try to obtain a more suitable form for these equations by writing them in Lagrangian form. Let us first define for $-1\leqslant\theta\leqslant 1$

$$\mathbf{m}_\theta=\boldsymbol{\Omega}(\mathbf{u})+\theta\mathbf{D}(\mathbf{u})=\tfrac{1}{2}[(1+\theta)\nabla u-(1-\theta)\nabla\mathbf{u}^{\mathrm{T}}]. \tag{29}$$

We can thus rewrite (16) in the form

$$\frac{\delta_\theta \mathscr{T}}{\delta t} = \frac{\partial \mathscr{T}}{\partial t} + \mathbf{u}\cdot\nabla\mathscr{T} + \mathscr{T}\mathbf{m}_\theta + \mathbf{m}_\theta^{\mathrm{T}}\mathscr{T}. \tag{30}$$

Let then $\mathbf{X}(\mathbf{x}, t; s)$ be the position at time s of a particle located at $\mathbf{x}$ at time t. We thus have

$$\left.\begin{aligned} &\frac{\partial X}{\partial s}(\mathbf{x}, t; s) = \mathbf{u}(\mathbf{X}(\mathbf{x}, t, s), s), \\ &\mathbf{X}(\mathbf{x}, t, t) = \mathbf{x}. \end{aligned}\right\} \tag{31}$$

We also define the following tensor-valued function that describes the history of the deformation tensor:[4,9]

$$\left.\begin{aligned} &\mathbf{F}(\mathbf{x}, t; s) = \nabla_{\mathbf{x}}\mathbf{X}(\mathbf{x}, t; s), \\ &\mathbf{F}(\mathbf{x}, t; t) = \mathbf{I}. \end{aligned}\right\} \tag{32}$$

One then checks[4] that $\mathbf{F}$ is the solution of the differential system

$$\left.\begin{aligned} &\frac{\partial \mathbf{F}}{\partial t}(\mathbf{x}, t; s) = \mathbf{u}(\mathbf{x}, t)\cdot\nabla_{\mathbf{x}}\mathbf{F}(\mathbf{x}, t; s) - \mathbf{F}(\mathbf{x}, t; s)\nabla_{\mathbf{x}}\mathbf{u}(x, t), \\ &\mathbf{F}(\mathbf{x}, t; t) = \mathbf{I}, \end{aligned}\right. \tag{33}$$

or, introducing the material derivative

$$\left.\begin{aligned} &\frac{\mathrm{D}\mathbf{F}}{\mathrm{D}t} = \frac{\partial \mathbf{F}}{\partial t} + \mathbf{u}\cdot\nabla\mathbf{F}, \\ &\frac{\mathrm{D}\mathbf{F}}{\mathrm{D}t} = -\mathbf{F}\nabla\mathbf{u}(\mathbf{x}, t) \end{aligned}\right\} \tag{34}$$

It is then a simple exercise to check that we have

$$\left.\begin{aligned} &\frac{\mathrm{D}\mathbf{F}^{-\mathrm{T}}}{\mathrm{D}t} = \mathbf{F}^{-\mathrm{T}}(\nabla\mathbf{u})^{\mathrm{T}}, \\ &\mathbf{F}^{-\mathrm{T}}(\mathbf{x}, t; t) = \mathbf{I}, \end{aligned}\right\} \tag{35}$$

where $\mathbf{F}^{-\mathrm{T}} = (\mathbf{F}^{-1})^{\mathrm{T}}$, as usual.

Let us now consider a differential system containing both (34) and (35) as special cases. We define $\mathbf{R}_\theta(\mathbf{x}, t; s)$ to be the solution of

$$\left.\begin{aligned} &\frac{\mathrm{D}\mathbf{R}_\theta(\mathbf{x}, t; s)}{\mathrm{D}t} = \mathbf{R}_\theta(\mathbf{x}, t; s)\mathbf{m}_\theta^{\mathrm{T}}(\mathbf{x}, t), \\ &\mathbf{R}_\theta(\mathbf{x}, t; t) = \mathbf{I}. \end{aligned}\right\} \tag{36}$$

For $\theta = -1$ and $\theta = +1$ we get back (34) and (35), respectively. For $\theta = 0$ we have, setting $\mathbf{R} = \mathbf{R}_0$

$$\frac{\partial \mathbf{R}}{\partial t}(\mathbf{x}, t; s) = -\mathbf{R}(\mathbf{x}, t; s)\,\boldsymbol{\Omega}(\mathbf{u}), \tag{37}$$

and we take into account only the rotation part of the deformation. Defining now,

$$\mathbf{W}_\theta(\mathbf{x}, t; s) = \mathbf{R}_\theta(\mathbf{x}, t; s)\boldsymbol{\sigma}(\mathbf{x}, t)\mathbf{R}_\theta^{\mathrm{T}}(\mathbf{x}, t; s), \tag{38}$$

it is then a matter of tedious calculations to obtain from (38) and (36)

$$\frac{\partial \mathbf{W}_\theta}{\partial t}(\mathbf{x}, t; s) + \mathbf{u}(\mathbf{x}, t)\cdot\nabla \mathbf{W}_\theta(\mathbf{x}, t; s) = \mathbf{R}_\theta(\mathbf{x}, t; s)\frac{\delta_\theta \boldsymbol{\sigma}}{\delta t}(\mathbf{x}, t)\mathbf{R}_\theta^{\mathrm{T}}(\mathbf{x}, t; s). \tag{39}$$

Using (39) our constitutive law (27) can be transformed as

$$\lambda_1 \frac{\mathrm{D}\mathbf{W}_\theta}{\mathrm{D}t}(\mathbf{x}, t; s) = 2\eta_1 \mathbf{R}_\theta(x, t; s)\mathbf{D}\mathbf{u}(\mathbf{x}, t)\mathbf{R}_\theta^{\mathrm{T}}(\mathbf{x}, t; s) - \hat{Y}(\varepsilon, \mathbf{W}_\theta)\mathbf{W}_\theta(\mathbf{x}, t; s), \tag{40}$$

where $\hat{Y}(\varepsilon, \mathbf{W}_\theta) = Y(\varepsilon, \boldsymbol{\sigma}) = Y(\varepsilon, \mathbf{R}_\theta^{-1}\mathbf{W}_\theta\mathbf{R}_\theta^{-\mathrm{T}})$.

A numerical scheme for viscoelastic constitutive laws

Although the finite element that we propose will ultimately be founded on a weak formulation of the transport equation, we shall first consider, to fix ideas, a simple discretization of (36) and (40). Let us suppose for the moment that $\mathbf{u}(\mathbf{x}, t)$ is a given vector field; let also $\boldsymbol{\sigma}$ be known at time t_n, whereas we want to find its values at time $t_{n+1} = t_n + \Delta t$.
We first approximate $X(x, t_{n+1}, t_n)$ by

$$\mathbf{x}_* = \mathbf{x} - \mathbf{u}(\mathbf{x}, t_{n+1})\Delta t, \tag{41}$$

that is we approximate the particle path by a straight line (Figure 3). We then apply along this path a simple Euler's scheme to (36):

$$\frac{\mathbf{R}_\theta(\mathbf{x}, t_{n+1}, t_{n+1}) - \mathbf{R}_\theta(\mathbf{x}_*, t_n; t_{n+1})}{\Delta t} = \mathbf{R}_\theta(\mathbf{x}, t_{n+1}, t_{n+1})\mathbf{m}_\theta^{\mathrm{T}}(\mathbf{x}, t_{n+1}), \tag{42}$$

which yields, as $\mathbf{R}_\theta(\mathbf{x}, t, t) = \mathbf{I}$,

$$\mathbf{R}_\theta(\mathbf{x}_*, t_n, t_{n+1}) = \mathbf{I} - \Delta t\mathbf{m}_\theta^{\mathrm{T}}(\mathbf{x}, t_{n+1}). \tag{43}$$

This enables us to compute

$$\mathbf{W}_\theta(\mathbf{x}_*, t_n, t_{n+1}) = \mathbf{R}_\theta(\mathbf{x}_*, t_n, t_{n+1})\boldsymbol{\sigma}(\mathbf{x}_*, t_n)\mathbf{R}_\theta^{\mathrm{T}}(\mathbf{x}_*, t_n, t_{n+1}), \tag{44}$$

so that we can again use a simple Euler's scheme on (40) to obtain

$$\lambda_1 \frac{\mathbf{W}_\theta(\mathbf{x}, t_{n+1}, t_{n+1}) - \mathbf{W}_\theta(\mathbf{x}_*, t_n, t_{n+1})}{\Delta t} = 2\eta_1 \mathbf{R}_\theta(\mathbf{x}, t_{n+1}, t_{n+1})$$
$$\times \mathbf{D}\mathbf{u}(\mathbf{x}, t_{n+1})\mathbf{R}_\theta^{\mathrm{T}}(\mathbf{x}, t_{n+1}, t_{n+1}) - \hat{Y}(\varepsilon, \mathbf{W}_\theta(\mathbf{x}, t_{n+1}, t_{n+1}))\mathbf{W}_\theta(\mathbf{x}, t_{n+1}, t_{n+1}). \tag{45}$$

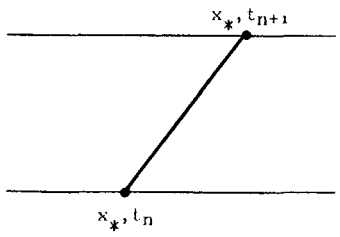

Figure 3.

This then reduces to

$$\lambda\frac{\boldsymbol{\sigma}(\mathbf{x},t_{n+1})-\mathbf{W}(\mathbf{x}_*,t_n,t_{n+1})}{\Delta t}+2\eta_1\mathbf{D}\mathbf{u}(\mathbf{x},t_{n+1})-Y(\varepsilon,\boldsymbol{\sigma}(\mathbf{x},t_{n+1}))\boldsymbol{\sigma}(\mathbf{x},t_{n+1}). \tag{46}$$

For $Y(\varepsilon,\boldsymbol{\sigma})=$ constant, this is a linear equation for $\boldsymbol{\sigma}(\mathbf{x},t_{n+1})$. In the general case we have a non-linear relation that must be solved by some iterative method.

Although this is the basic idea, it is not, as such, compatible with a finite element formulation. To fully present our numerical method for viscoelastic flows we shall therefore introduce a weak formulation of the transport equation.

A WEAK FORMULATION FOR THE TRANSPORT EQUATION

We briefly describe here a numerical method essentially due to Benque *et al.*[10] Let us suppose that we want to solve a transport problem

$$\frac{\partial T}{\partial t}+\mathbf{u}\cdot\nabla T=\mathbf{f}, \tag{47}$$

in a time-dependent domain $Q\subset\mathbb{R}^n\times(t_1,t_2)$, where $\mathbf{u}$ is a given divergence-free vector field and f a know external source. Let ϕ be a smooth enough test function (we shall not try here to develop a proper functional setting).

We multiply (47) by ϕ and integrate over Q to obtain the equivalent form:

$$\int_Q\left(\frac{\partial T}{\partial t}+\mathbf{u}\cdot\nabla T-f\right)\phi\,\mathrm{d}x\,\mathrm{d}t=0. \tag{48}$$

Following Figure 4, we denote by Ω_t the trace of Q at a fixed time t. In particular Ω_{t_1} and Ω_{t_2} are the initial and final configurations of Ω_t. We also denote by $\mathbf{n}_t$ the normal to $\partial\Omega_t$. We define $\Sigma=\cup_t\partial\Omega_t=\partial Q\backslash\Omega_{t_1}\backslash\Omega_{t_2}$. The normal to Σ makes an angle θ_t with the t-axis and an angle θ_x with the vector $\mathbf{n}_t$. We now integrate (48) by parts to obtain for any ϕ

$$-\int_Q T\left(\frac{\partial\phi}{\partial t}+\mathbf{u}\cdot\nabla\phi\right)\mathrm{d}x\,\mathrm{d}t+\int_{\Omega_{t_2}}T\phi\,\mathrm{d}x-\int_{\Omega_{t_1}}T\phi\,\mathrm{d}x$$
$$+\int_\Sigma(\mathbf{n}\cdot\mathbf{n}_t T\phi\cos\theta_x+T\phi\cos\theta_t)\,\mathrm{d}\theta=\int_Q f\phi\,\mathrm{d}x\,\mathrm{d}t. \tag{49}$$

In order to employ (49), we shall now make two special choices that will greatly simplify it:

1. We take Σ parallel to the velocity field $\mathbf{u}$ (that is we follow the characteristics). This means,

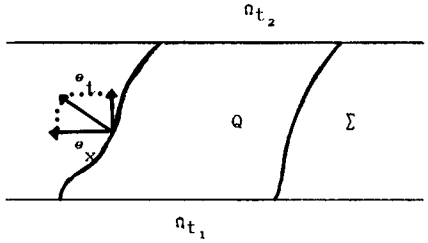

Figure 4.

$$\mathbf{u}\cdot\mathbf{n}\cos\theta_x + \cos\theta_t = 0, \quad \text{on} \quad \Sigma. \tag{50}$$

2. We take ϕ satisfying

$$\frac{\partial\phi}{\partial t} + \mathbf{u}\cdot\nabla\phi = 0. \tag{51}$$

Equation (49) then reduces to

$$\int_{\Omega_{t_2}} T\phi\,\mathrm{d}x - \int_{\Omega_{t_1}} T\phi\,\mathrm{d}x = \int_{Q} f\phi\,\mathrm{d}x\,\mathrm{d}t, \quad \forall\phi. \tag{52}$$

If one knows $T_1 = T|_{\Omega_{t_1}}$ and f, (52) enables one to compute $T_2 = T|_{\Omega_{t_2}}$. This is nothing but a week form of the method of characteristics. It must be noted here that (51) implies that ϕ is completely determined by its value on Ω_{t_2}.

We shall now consider a finite element simple implementation of (51) and (52). We consider on Ω a finite element mesh $\mathscr{T}_h$ of triangles or quadrilaterals. We approximate T by the usual technique of the finite element method, that is for any $K\in\mathscr{T}_h$ we define an approximation T_n, such that

$$T_n|_K = \hat{T}_h \circ G_K, \tag{53}$$

where $\hat{T}_n\in\hat{P}\subset P_1(\hat{K})$ is a polynomial function on a reference element and $\hat{K}$ and G_K is the transformation that maps $\hat{K}$ onto K. We require no continuity at interfaces.

Supposing $\mathbf{u}$ to be known, we compute the domain generated by the characteristics emanating from K. In practice this means computing the characteristics emanating at time t_2 from the geometric nodes of K. (Figure 5). In general the image K_{t_1} at time t_1 of K will be a general

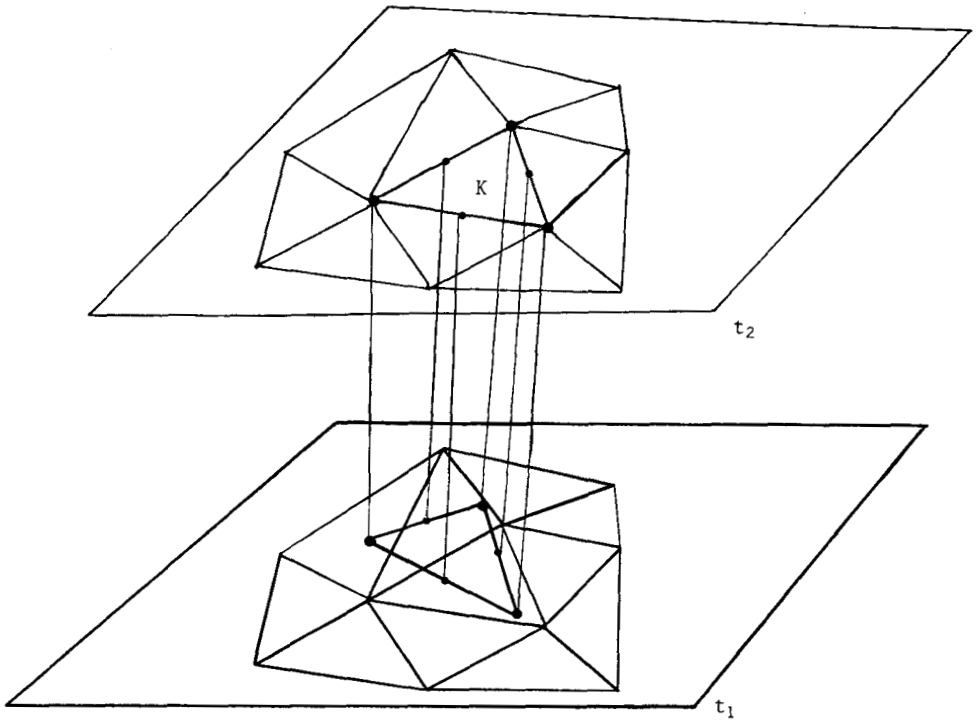

Figure 5.

isoparametric element, even if K is a straight-sided element. Moreover we consider a basis $\{w_i\}$ for $\hat{\phi}$ and we use a set of test functions satisfying (51) and such that

$$\phi_i(t) = w_i \circ G_K(t). \tag{54}$$

Computing T_2, when T_1 and f are known, is then a matter of solving a small linear system. It is even generally possible to choose w_i in order that $\phi_i|_{K_{t_2}}$ forms an orthogonal basis for the $L_2(K)$ scalar product, so that the system (52) becomes diagonal. This is indeed readily achieved by using Lagrange interpolation functions associated with a set of Gaussian nodes. On a quadrilateral, it is direct to define a biquadratic element by its value on the nine points of a standard product formula.

Whenever this is done, integration in x at a fixed t reduces to a simple sum. If we take in (52) ϕ to be the test function associated with a quadrature node this sum reduces to one point, as ϕ vanishes on other quadrature points.

Moreover, we have chosen to approximate the time integral by a one-point rectangle formula:

$$\int_{t_1}^{t_2} f(t)\,\mathrm{d}t = (t_2 - t_1) f(t_2). \tag{55}$$

The approximation of (52) then breaks down into a very simple procedure, namely an implicit Euler's scheme on every quadrature point x_i:

$$T_2(x_i) = T_1(\mathbf{X}(\mathbf{x}_i, t_2, t_1) + (t_2 - t_1) f(x_i)). \tag{56}$$

Applying this procedure to (40) at every quadrature point $\mathbf{x}_i$ in K and approximating $\mathbf{X}(\mathbf{x}_i, t_2, t_1)$ by the scheme (41), one obtains precisely Euler's scheme (46). Applying it at every Gaussian node thus yields an approximation of the weak formulation. Furthermore, computing $\boldsymbol{\sigma}$ at Gaussian nodes is precisely what is needed in the finite element code to compute the integrals, such as

$$\int_K \boldsymbol{\sigma} : \mathbf{D}(\mathbf{v})\,\mathrm{d}x, \tag{57}$$

arising from the weak form of div $\boldsymbol{\sigma}$.

APPROXIMATION AND SUMMARY OF THE NUMERICAL PROCEDURE

We now summarize the numerical technique coming out of the previous developments, when applied to a discretized version of (24)–(28). We shall use here the same finite element approximation of the velocity and pressure field as we used in the section on 'Generalized Newtonian flows', that is the now standard $Q_2 - P_1$ biquadratic-velocity linear-pressure element. Again we require here that in the limiting Newtonian case one should obtain a standard approximation of the Navier–Stokes equations. This can again be obtained by using a discontinuous biquadratic element to approximate $\boldsymbol{\sigma}_1$. From the previous section, one is led to use as degrees of freedom of this element the point values of the extra stress at nine Gaussian modes on each quadrilateral.

The problem that we want to solve is a time-dependent problem, and we shall describe here how one time step can be computed. We thus suppose that quantities $\mathbf{u}$ and $\boldsymbol{\sigma}_1$ are known at time t_n and we denote these values by $\mathbf{u}^n$ and $\boldsymbol{\sigma}_1^n$. (These are of course discrete values.) We now want to compute new values at time t_{n+1}; to do so we have to solve a non-linear system and some kind of iterative procedure has to be used. At the present time this has been a simple fixed-point procedure, but more elaborate, and it is hoped more efficient, methods are under test.

The time stepping needed to solve (24)–(28) was performed by a simple *implicit* Euler's scheme.

From (24), (26) and (28) one then obtains

$$\rho\left(\frac{\mathbf{u}^{n+1}-\mathbf{u}^n}{\Delta t}+\mathbf{u}^{n+1}\cdot\nabla\mathbf{u}^{n+1}\right)-2\eta_2\,\mathrm{div}\,\mathbf{D}(\mathbf{u}^{n+1})-\mathrm{div}\,\boldsymbol{\sigma}_1^{n+1}+\nabla p^{n+1}=\rho\,\mathbf{f}. \tag{58}$$

Whenever $\boldsymbol{\sigma}_1^{n+1}=0$, this is a classical discretization of the Navier–Stokes problem. In order to use (58) we now need some technique to extract $\boldsymbol{\sigma}_1^{n+1}$ out of the available data. To do so, we approximate (27) by the weak formulation of the previous section and the form (40) of the constitutive equation. We start from some initial guess for $\mathbf{u}^{n+1}$ (e.g. $\mathbf{u}^{n+1}=\mathbf{u}^n$) and we apply (41), (43), (44) and (46) at each Gaussian node of each element. The only difficulty is to evaluate $\boldsymbol{\sigma}_1(\mathbf{x}_n,t_n)$ at the point $\mathbf{x}_*=\mathbf{x}-\mathbf{u}^{n+1}\Delta t$. We used the following technique.

The characteristics from the nine *geometric* nodes of the element are computed (cf. Figure 5) and we identify in which element they lie at time t_n. From this we obtain at time t_n a full isoparametric element and we compute the values of $\boldsymbol{\sigma}_1$ at its nodes by interpolating from the values on the fixed mesh. (This implies of course some numerical diffusion.) Whenever the node falls on a point where the approximation of $\boldsymbol{\sigma}_1^n$ on the fixed mesh is not continuous, we use the *upwind* value. From this new isoparametric interpolation we can compute any value we need at the Gaussian nodes.

We then obtain from (46), using a semi-implicit discretization for the eventual non-linear term $Y(\varepsilon,\boldsymbol{\sigma})\boldsymbol{\sigma}$,

$$\boldsymbol{\sigma}_1^{n+1}=\frac{2\eta_1\Delta t}{\lambda+Y(\varepsilon,\boldsymbol{\sigma}_1^n)\Delta t}=\mathbf{D}(\mathbf{u}^{n+1})+\frac{\lambda}{\lambda+Y(\varepsilon,\boldsymbol{\sigma}_1^n)\Delta t}\mathbf{W}_\phi^n. \tag{59}$$

Substituting this expression into (58) yields

$$\rho\left(\frac{\mathbf{u}^{n+1}-\mathbf{u}^n}{\Delta t}+\mathbf{u}^{n+1}\cdot\nabla\mathbf{u}^{n+1}\right)-2\left(\eta_2+\frac{\eta_1\Delta t}{\lambda+Y(\varepsilon\cdot\boldsymbol{\sigma}_1^n)\Delta t}\right)$$
$$\times\,\mathrm{div}\,\mathbf{D}(\mathbf{u}^{n+1})-\frac{\lambda}{\lambda+Y(\varepsilon\cdot\boldsymbol{\sigma}_1^n)\Delta t}\mathrm{div}\,\mathbf{W}_\theta^n+\nabla p^{n-1}=\rho\mathbf{f}. \tag{60}$$

This means that we have essentially to solve a Navier–Stokes problem with a modified viscosity term and an additional term (div $\mathbf{W}_\theta^n$) on the right-hand side. This problem was solved by a standard Newton–Raphson method, embedded in a fixed-point algorithm: given $\mathbf{u}^{n+1}$, one computes $\mathbf{W}_\theta^n$, from which $\mathbf{u}^{n+1}$ is recomputed, etc. The convergence of this fixed-point procedure can be modulated by the choice of the time-step. We found that a convenient number of iterations was 4 or 5. A larger number was often the sign that a rapid variation of the solution could not adequately followed by the time-stepping procedure.

NUMERICAL RESULTS

The method described in the previous sections being relatively new, it is not possible to present a complete set of results for all possible cases. We however believe that there is some evidence that we have been able to make visible a few phenomena that had escaped previous computations. The results presented here come from a simple Maxwell model, that is $Y(\varepsilon,\boldsymbol{\sigma})\equiv 1$, $\lambda_2=0$, $\theta=\pm 1$. Even if the solution is not the same for the contravariant ($\theta=-1$) and the covariant ($\theta=+1$) models, the phenomena described below were observed in both cases, and we shall make no distinction unless the contrary is stated explicitly.

We essentially computed results in two geometries, both of academic nature. The first one was a 'Poiseuille' flow, that is a developed flow between two parallel plates. As an exact solution

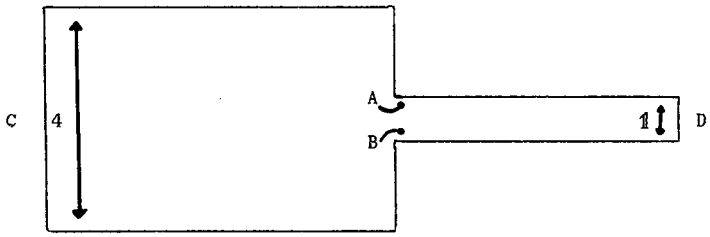

Figure 6.

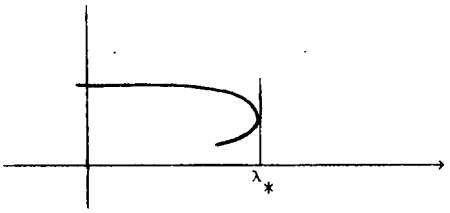

Figure 7.

is known in this case this was a check that the code did not contain some tragic mistake. It was indeed possible to compute the exact solution upto an error in Δt coming from the Euler's scheme used for the time-stepping procedure (the space discretization was rich enough not to introduce errors). The second one a 4:1 contraction (Figure 6). This problem has become a kind of bench-mark, and comparison with previous computations permits evaluation of the performance of new ones. It is a difficult problem: the stresses are strongly singular near the corners A and B (see for instance Reference 11). This is likely to generate strange behaviour in this region because of the memory properties of a viscoelastic flow: the influence of the singularity will be extended downstream. The boundary conditions were a developed flow on C and a free exit at D. This problem is obviously symmetric with respect to the central axis of the contraction, and it is natural to compute on a half-domain by forcing the symmetry explicitly. As we shall see, this may hide some important phenomena and should be avoided.

The main issue in this contraction problem is the so-called 'high Weissemberg number problem'. The phenomenon is the following: there exists a critical value λ_* of λ_1 beyond which *no steady-state solution* can be found. Continuation methods have shown this to correspond to a turning point[12] (Figure 7) and not for instance to a Hopf bifurcation towards some periodic solution. This phenomenon corresponds to the half contraction symmetric geometry (or to an axisymmetric three-dimensional geometry). Our numerical method, being essentially time-dependent, could compute steady-state solutions only by the convergence of a time dependent process. Our results confirmed the above-described observations: we were unable to converge beyond some λ_*. Moreover, the time-dependent problem then exploded, showing that we had not bifurcated to some unsteady phenomenon.

While analysing these results we were however led to believe that the non-convergence was developing around the axis of symmetry. To analyse this phenomenon more clearly and to avoid any possible mistake in taking into account symmetry we built a mesh for the complete contraction.

The situation then *changed radically*: we were not able to obtain any steady-state solution for any Weissemberg number, however small. Instead we observed the appearance of a *non-spatially-*

symmetric periodic solution. This could of course not be computed by a steady-state method in a half domain.

We no longer had a high Weissemberg number problem, but rather a small Weissemberg number problem: the solution was harder to converge inside each time step for small values of λ_1. This paradoxical phenomenon can be understood when one realizes that the period of the solution is roughly $O(\sqrt{\lambda_1})$. Thus oscillations get shorter and shorter for small λ_1 and a smaller time step is needed to represent them adequately. This is consistent with the *singular limit* character of the case $\lambda_1 = 0$: the memory phenomenon of the model implies a memory fading like e^{-t/λ_1} along streamlines.

The question that now arises is whether this periodic oscillatory solution makes any sense. It is indeed a reasonable suspicion that it could be generated by the numerical method.

Let us first get rid of a possible trouble, namely changes of type. It is known[13,14] that the equations of viscoelastic fluids can present changes of type, and that hyperbolic pockets can develop, analogous to supersonic pockets in transonic flows. However when one neglects inertial terms in (24), it can be proved that this change of type cannot occur. In this case it is very simple to see that an artificial change of type would occur if the determinant of $(\boldsymbol{\sigma} - \lambda \mathbf{I})$ were to become negative. This is easy to check, and we were able to verify that no change of type had occurred in our computations.

On the other hand, the theoretical results of Joseph[14] are consistent with our computations. There is in fact a damped wave equation underlying the viscoelastic model in the small perturbation case and it is surely possible to think that in the general case vorticity waves are generated by some non-linear mechanism. Moreover, symmetry breaking is a quite a common phenomenon in non-linear elasticity, and it is not a surprise to see symmetric date generate a non-symmetric behaviour.

What kind of bifurcation diagram could explain or describe this phenomenon? It is easy to see that $\lambda = 0$ is not a Hopf bifurcation point in the standard sense of Figure 8. The Stokes problem is a symmetric problem with real eigenvalues. Therefore some other form should be sought. We conjecture that the diagram of Figure 9 could be used to describe our problem. A periodic branch appears from infinity at $\lambda = 0$. This is compatible with the singular limit property of $\lambda = 0$. A steady branch still exists for $\lambda > 0$, at least for $\lambda < \lambda_*$. It is probably unstable and is

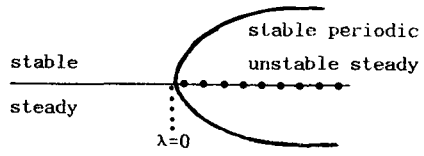

Figure 8.

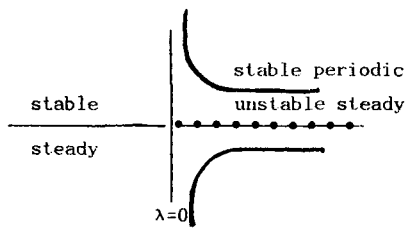

Figure 9.

computed only by careful continuation or because it is made stable by numerical dissipation. Such a branch could even be a purely numerical artefact, if one takes into account the results of Keunings,[12] who showed that the critical value of λ gets smaller and smaller when fine meshes are used.

Of course this is purely conjectural. We, however, believe that such an explanation is worth a verification and we are at present working on another numerical procedure that could possible cross-check what we presented here.

Let us now come to the results themselves. Where do these oscillations take place? As we might expect it is near the neck of the contraction, where singularities are likely to produce strong effects. Figures 10 and 11 show Lissajou's diagrams (v_2 vs. u_1) of the velocities at

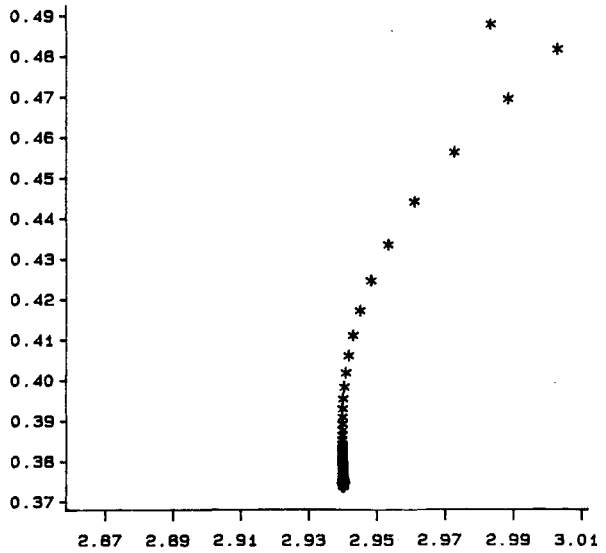

Figure 10.

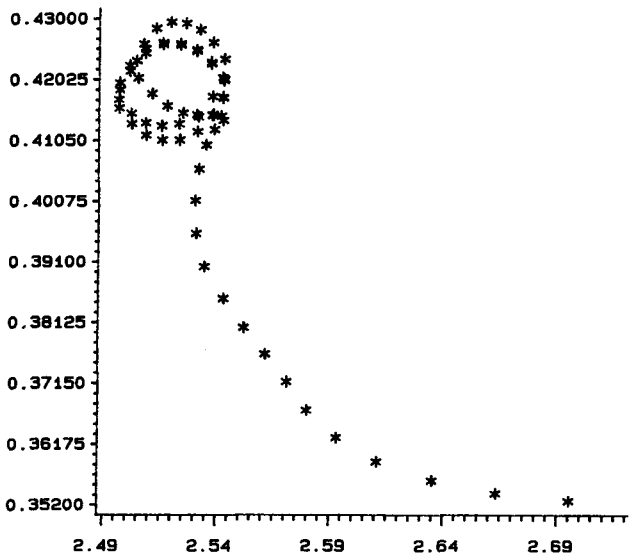

Figure 11.

point A of Figure 6, for $\lambda_1 = 0$ and $\lambda_1 = 0{\cdot}1$, respectively, as a function of time. For $\lambda = 0$ we have convergence and data accumulate to a limit point. For $\lambda = 0{\cdot}1$ the periodic behaviour is clearly visible and it corresponds to a pulsation in the velocity field that grows up to a local periodic flow for λ_1 large enough. (It must be noted that our numerical method guarantees mass conservation, so that the total flow in the neck is always accurate.) A further point in favour of

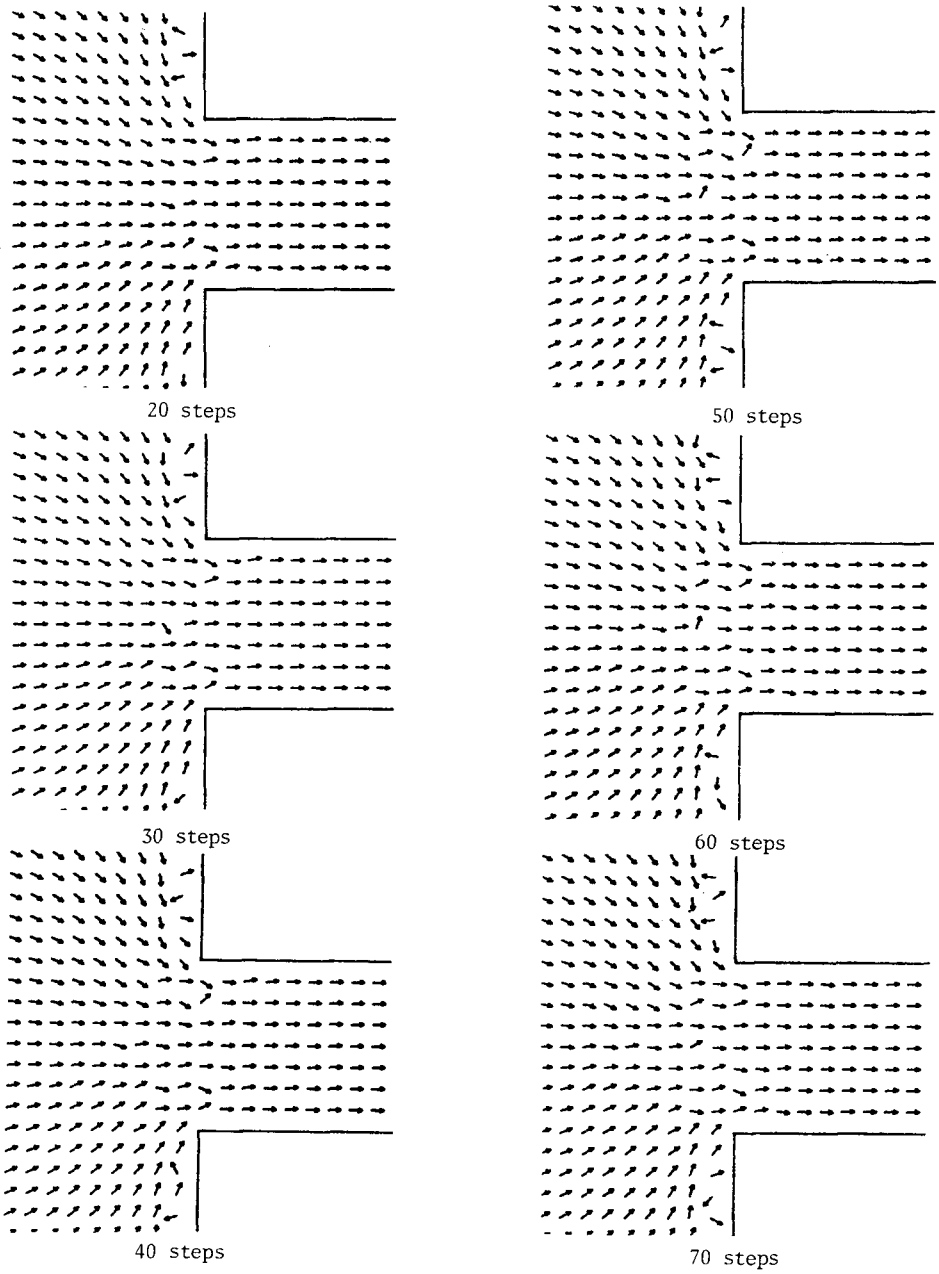

Figure 12.

the significance of these numerical results is that such pulsations near the neck *have been observed experimentally* by researchers of the Institut de Mécanique de Grenoble.

In Figure 12 we present a sequence of flow fields for $\lambda_1 = 0{\cdot}3$ showing how the flow actually oscillates.

Finally we show how the σ_{12} component of the stress tensor is non-symmetric as λ_1 grows. Figures 13 and 14 present σ_{12} for $\lambda = 0{\cdot}1$ at two different time steps separated by approximatively one period of the periodic oscillation. One sees near the neck nearly anti-symmetric values. It must be said that this could never be detected by looking at streamlines, which are not perturbed in a visible way.

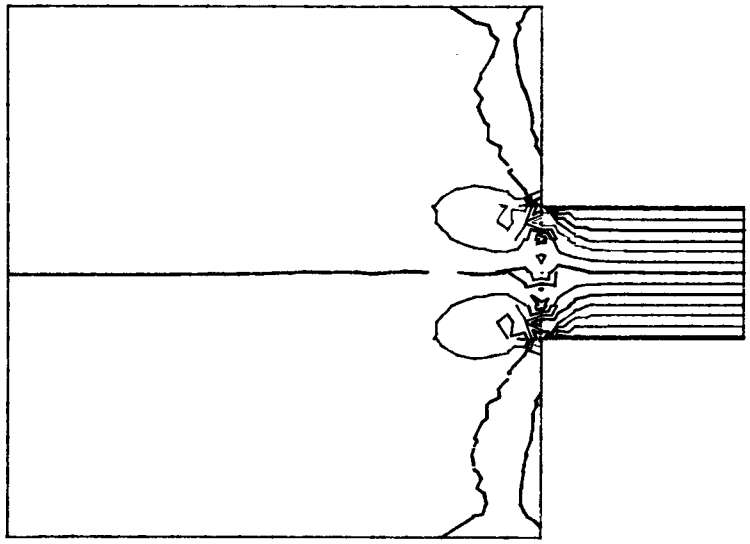

Figure 13.

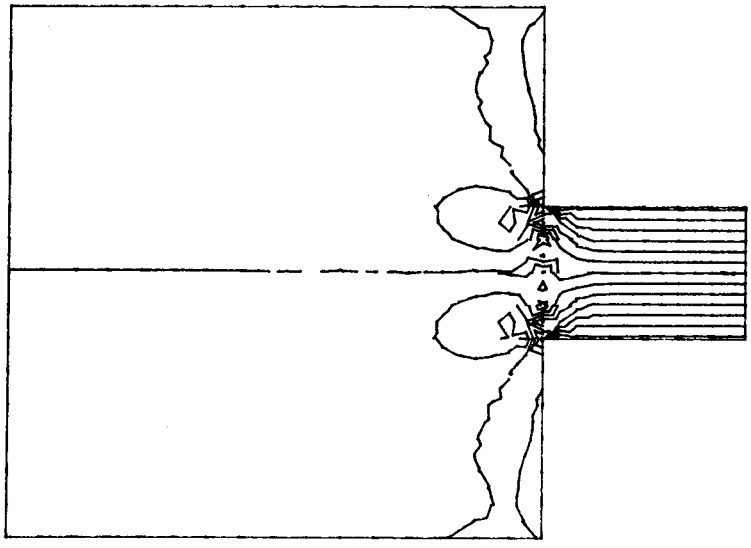

Figure 14.

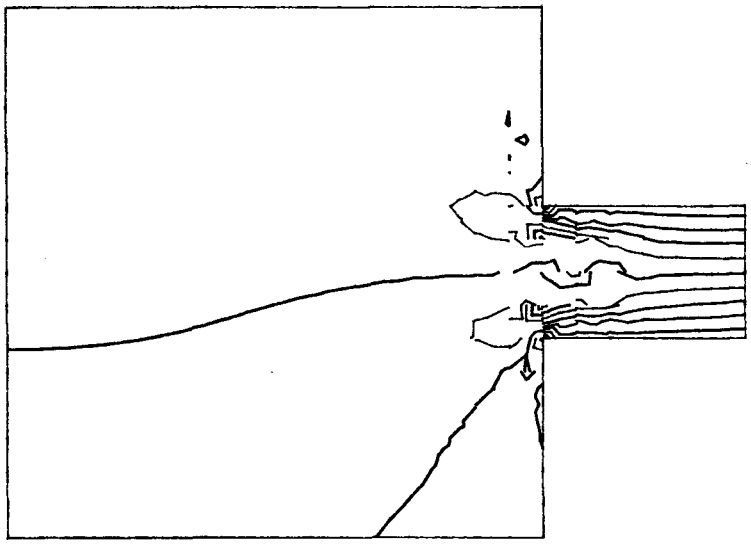

Figure 15.

Figure 15 shows σ_{12} for $\lambda_1 = 0{\cdot}3$, where non-symmetry has grown rather strongly.

CONCLUSION

Numerical solution of viscoelastic materials is a hard problem. Our aim in the present study was to see if new numerical methods could produce significant results and circumvent difficulties such as the high Weissemberg number problem. We have at least obtained results that suggest a new explanation for this phenomenon, and the numerical method developed has proved to be manageable. There remain many open questions and we intend to verify our conjecture through other numerical procedures and by further comparison with experimental results.

REFERENCES

1. M. J. Crochet, A. R. Davies and K. Walters, *Numerical Simulation of Non-Newtonian flows*, Elsevier, Amsterdam, 1984.
2. Ph. Tanguy, M. Fortin and L. Choplin, 'Finite element simulation of dip coating. II: Non-Newtonian fluids', *Int. J. numer. methods Fluids*, **4**, 459–475 (1984).
3. M. Fortin, and R. Glowinski, *Résolution Numérique de Problèmes aux Limites par des Méthodes de Lagrangien Augmenté*, Dunod, Paris, 1983.
4. R. B. Bird, R. C. Armstrong and O. Hassager, *Dynamics of polymetric Liquids, Vol. I, Fluid Mechanics*, Wiley, New York, 1977.
5. R. Darby, *Viscoelastic Fluids, An Introduction to Their Properties and Behaviour*, M. Dekker, 1976.
6. B. D. Coleman and W. Noll, 'Foundations of linear viscoelasticity', *Rev. Mod. Physics*, **33**, 239–249 (1961); Erratum: *op. cit.*, **36**, 1103 (1964).
7. N. Phan Thien and R. I. Tanner, 'A new constitutive equation derived from network theory', *J. Non-Newt. Fluid Mech.*, **2**, 353–365 (1977).
8. R. Keunings and M. J. Crochet, 'Numerical simulation of the flow of a viscoelastic fluid through an abrupt contraction', *J. Non-Newt. Fluid Mech.*, **14**, 279–299 (1984).
9. J. E. Marsden and T. J. R. Hughes, *Mathematical foundations of Elasticity*, Prentice-Hall, 1983.
10. J. P. Benque, G. Labadie and J. Ronat, 'A finite element method for Navier–Stokes equations coupled with a temperature equation', *Proceedings of the 4th Internal Symposium on finite elements in flow problems*, Tokyo, Japan, 1982.
11. G. G. Lipscomb, R. Keunings and M. M. Deen, 'Implications of boundary singularities in complex geometries', submitted to *J. Non-Newt. Fluid Mech.*
12. R. Keunings, 'On the high weissemberg number problem', *J. Non-Newt. Fluid Mech.*, **20**, 209–226 (1986).

13. D. D. Joseph, M. Renardy and J. C. Saut, 'Hyperbolicity and change of type in the flow of viscoelastic fluids', *MRC Technical Summary Report* τ2657, Mathematics Research Center, Madison, Wisconsin, 1984; *Arch. Rational Mech. Anal.*, **87**, (3), 213–251 (1985).
14. D. D. Joseph, 'Hyperbolic phenomena in the flow of viscoelastic fluids', *Lecture Presented at the Symposium on Viscoelasticity and Rheology*, Mathematics Research Center, Madison-Wisconsin, 16–18 October 1984.
15. M. J. Crochet and R. Keunings, 'Finite element analysis of die swell of a highly elastic fluid', *J. Non-Newt. Fluid Mech.*, **10**, 339–356 (1982).